Journal of Zhejiang University SCIENCE
ISSN 1009-3095
http://www.zju.edu.cn/jzus
E-mail: jzus@zju.edu.cn

Electrode models in electrical impedance tomography

WANG M.
(*Institute of Particle Science and Engineering, University of Leeds, LS2 9JT, UK*)
E-mail: m.wang@leeds.ac.uk

Received Aug. 26, 2005; revision accepted Sept. 15, 2005

Abstract: This paper presents different views on electrode modelling, which include electrode electrochemistry models for modelling the effects of electrode-electrolyte interface, electric field electrode models for modelling electrode geometry, and electrode models for modelling the effects of electrode common mode voltage and double layer capacitance. Taking the full electrode models into consideration in electrical impedance tomography (EIT) will greatly help the optimised approach to a good solution and further understanding of the measurement principle.

Key words: Electrical impedance tomography (EIT), Electrochemistry, Electrode modelling
doi:10.1631/jzus.2005.A1386 **Document code:** A **CLC number:** TB126

INTRODUCTION

This paper presents different views on electrode modelling in electrical impedance tomography (EIT), which include electric field electrode models—the conventional approach for modelling electrode geometry, electrochemistry electrode models for modelling the effects of electrode-electrolyte interface, and the electrode measurement models for modelling the sensing system in the terms of the electronic measurements. Taking the full electrode models into consideration of electrical impedance tomography leads to further understanding of the measurement principle.

ELECTROCHEMISTRY MODELS

Overpotential-current relation

A metal electrode immersed in an electrolyte is polarised when its potential is different from its open-circuit potential (Weinman and Mahler, 1964). The difference between the open circuit potential V_e (equilibrium potential) and the actual potential V is the overpotential, η. Relating the net current density, j, of the electrochemical reaction to the overpotential described by the Butler-Volmer equation (Bockris and Drazic, 1972) is given in Eq.(1).

$$j = j_0\{\exp[(1-\beta)F\eta/GT] - \exp(-\beta F\eta/GT)\} \quad [\mathrm{A/cm^2}] \tag{1}$$

where j_0 is known as the exchange current density and a function of the metal-electrolyte system and, to a limited extent, of the surface structure of the metal. As an example, for a platinum electrode immersed in 75 Ω·cm resistivity saline, j_0 is in the order of 5×10^{-5} A/cm^2 (Pollak, 1974b). F is the Faraday constant (96500 C/mol), G is the gas constant (8.317 J/(K·mol)), T is the temperature in Kelvin (298 K at room temperature), β is a factor close to 0.5 and related to the electrical energy passage involved during of the ion across the electrode-electrolyte interface (Bockris and Drazic, 1972).

For small overpotentials (−5 mV<η<5 mV) the relation between overpotential and current density is linear as given by Eq.(2) and illustrated in Fig.1a. The limits of linearity in Eq.(2) are typically reached at current density levels of up to 1 mA/cm^2 when a direct current is applied (Weinman and Mahler, 1964; Schwan and Ferris, 1968).

$$\eta = \frac{GT}{j_0 F} j \tag{2}$$

The relation approximates to a simpler form in special cases. Particularly when overpotentials are greater than 50 mV or less than −50 mV, the relation between overpotential and current density is described by a simpler Eq.(3) as shown in Fig.1b.

$$\eta = a + b \ln j \quad [\mathrm{V}] \tag{3}$$

where $a = -\dfrac{GT}{(1-\beta)F}$; $b = \dfrac{GT}{(1-\beta)F}$.

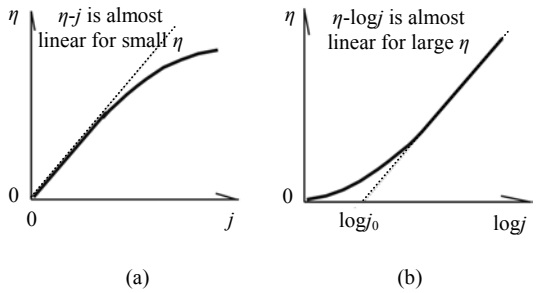

Fig.1 (a) For small overpotentials; (b) For large overptentials

Charge transfer resistance

By analogy with Ohm's Law ($V=IR$) the gradient of the η-j line in Fig.1 can be interpreted as the equivalent resistance per unit area, R_C, of the charge-transfer process on the electrode as given in Eq.(4) and which is called the charge transfer resistance for small overpotentials.

$$R_C = \frac{\partial \eta}{\partial j} = \frac{GT}{j_0 F} = \frac{E_T}{j_0} = \frac{0.026}{j_0} \qquad [\Omega \cdot \mathrm{cm}^2] \tag{4}$$

where E_T is called the temperature voltage. Its value at room temperature is approximately 0.026 V.

Since the exchange current density, j_0, and the charge transfer resistance per unit area R_C are inversely proportional in Eq.(4), the larger j_0 is, the smaller is R_C. When j_0 corresponds to the order of 5×10^{-5} A/cm^2, for the platinum electrode and 75 Ω·cm resistivity saline, R_C is approximately 500 Ω·cm^2 (Pollak, 1974b).

Double layer

Both theory and experiment confirm that the amount of charge stored in the region where the metal electrode is in contact with the electrolyte varies as a function of the potential difference across it (Bockris and Drazic, 1972; Crow, 1974). A simple model of the double layer was suggested by Helmhotz and Perrin at the end of the nineteenth century (Bockris and Conway, 1969; Bockris and Reddy, 1970). This represents the double layer in terms of the simple 'plates of a capacitor' point of view. The metal electrode, with its excess charge, forms one side of the double layer; and the electrolyte with its excess counter charge the other side of the double layer. Of course, there is no real plate on the electrolyte side, but it is imagined that the excess charges in the electrolyte make up a layer of charge just as if they were attached to a plate there (Bockris and Drazic, 1972). The Helmholtz double layer capacitance, C_H, is given by:

$$C_H = \frac{\mathrm{d}q_m}{\mathrm{d}V} = \frac{\varepsilon_r \varepsilon_0}{\delta^H} \qquad [\mu\mathrm{F/cm}^2] \tag{5}$$

In Eq.(5), q_m is the excess charge on the metal; V is potential across the double layer; ε_0 is the permittivity of a vacuum (8.85×10^{-8} μF/cm); ε_r is the relative permittivity of the material between the plates; δ^H is the effective distance between the plates ($\delta^H_{H_2O} = 2.8\times10^{-8}$ cm) (Bockris and Drazic, 1972). In reality, however, the double layer capacitance is not constant with potential and, for most electrode systems of practical importance, the capacitance in the absence of larger externally applied potential differences can be estimated to be about 10 μF/cm^2 (Pollak, 1974a) or 15.9 μF/cm^2 (Bockris and Drazic, 1972) irrespective of the ratio of the ions (Bockris and Reddy, 1970).

One approach to enhance the structure of the double layer was that of Gouy Chapman diffuse model (Bockris and Drazic, 1972), in which it was assumed that there would be no 'sticking' of ions to the electrode, and no contact adsorption, and suggested that the rigidity of Helmholtz theory, in which the excess charge on the solution was all placed in the same plane, and was all in contact with the electrode, should give place to a diffuse charge model. The diffuse capacitance is given in Eq.(6) by Crow (1974).

$$C_G = \varepsilon_r \varepsilon_0 \kappa = \frac{\varepsilon_r \varepsilon_0}{\delta^G} \tag{6}$$

where κ^{-1} is the effective radius of the ion atmosphere about an ion, here it is identified with δ^G the diffuse length of the double layer.

The total capacitance of the double layer, C, is made up of that due to the inner (adsorption) layer, C_H, and that due to the diffuse layer, C_G. Since these capacitances are connected in series:

$$\frac{1}{C} = \frac{1}{C_H} + \frac{1}{C_G} \quad \text{or} \quad C = \frac{C_H C_G}{C_H + C_G} \tag{7}$$

Consequently, if the electrolyte solution is very dilute, $C_G << C_H$ and $C \approx C_G$. The double layer is now essentially all diffuse. On the other hand, when the solution is very concentrated, $C_G >> C_H$ and $C \approx C_H$, which defines the Helmholtz's earliest model of the double layer.

Electrode-electrolyte equivalent circuit

An equivalent circuit of the electrode-electrolyte given by Pollak (1974b) is shown in Fig.2. The total impedance is made up of the interface part, the diffusion part and the inner resistance part, which are connected in series.

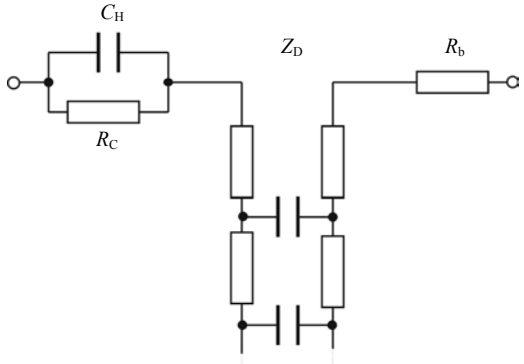

Fig.2 Equivalent circuit of the electrode-electrolyte impedance (R_C is the charge transfer resistance, C_H is the Helmhotz double layer capacitance, Z_D is the diffusion layer impedance, and R_b is the bulk resistance of the electrolyte)

Geddes *et al*.(1971) reported that when current density was increased up to 25 mA/cm^2, a definite non-linear behaviour was observed during their experiments at frequencies from 20 Hz to 10 kHz, which resulted in considerable distortion of the applied sine wave.

The response of the diffusion-layer to an a.c. current injection was given by Cobbold (1974) as:

$$Z_D \approx \frac{E_T}{z^2 c_0 F \sqrt{2\pi D} \cdot \sqrt{f}}(1 - j) \tag{8a}$$

$$|Z_D| \approx \frac{E_T}{z^2 c_0 F \sqrt{2\pi D}} \cdot \frac{1}{\sqrt{f}} \quad [\Omega \cdot \text{cm}^2] \tag{8b}$$

where D is the diffusion coefficient (cm^2/s), z the charge transfer number, c_0 the concentration of the electrolyte under equilibrium conditions (mol/cm^3).

For applications of the kind of electrolyte considered, for example the NaCl solution employed as the electrolyte, the diffusion coefficient is in the order of 1.5×10^{-5} cm^2/s and a charge transfer number in the order of 0.4 for the concentration below 0.2 mol/L of the NaCl solution can be expected (Conway, 1952). With these parameters the equation yields:

$$|Z_D| \approx \frac{7\times10^{-5}}{c_0\sqrt{f}} \quad [\Omega \cdot \text{cm}^2] \tag{9}$$

The above expression can be employed down to frequencies where the diffusion length δ^G becomes comparable with the electrode diameter d (Pollak, 1974a):

$$\delta^G = \sqrt{\frac{D}{2\pi f}} < d$$
$$f > \frac{D}{2\pi d^2} \approx \frac{8\times10^{-6}}{d^2} \quad [\text{Hz}]\ (d \text{ in cm}) \tag{10}$$

For the case of a concentration 1×10^{-5} mol/cm^3 at a frequency 100 Hz, $|Z_D|$=0.7 Ω·cm obtained from Eq.(9). Combining all of the above analyses, the total impedance, Z, of the electrode-electrolyte, at very low frequencies, is approximately equal to the diffusion-layer impedance Z_D (Cobbold, 1974; Pollak, 1974b):

$$Z \approx Z_D \propto 1/\sqrt{f} \tag{11}$$

and at very high frequency:

$$Z \approx R_b + \frac{1}{j\omega C_H} \quad [\Omega \cdot cm^2] \qquad (12)$$

In most applications, the effect of the diffusion-layer can be ignored in order to simplify the solution (Cobbold, 1974; Pollak, 1974a). The simplified equivalent circuit is given as shown in Fig.3.

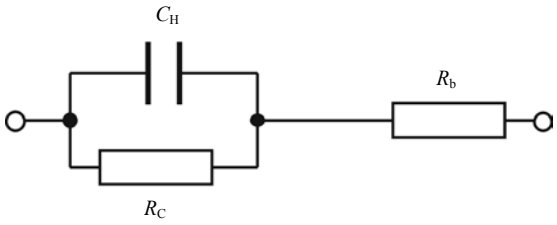

Fig.3 Equivalent circuit of the electrode-electrolyte impedance ignoring the diffusion effect

ELECTRIC FIELD MODELS

Bulk resistance

Suppose that the surface of the metal electrode in contact with the electrolyte is hemispherically shaped and that the radius of the process vessel is far larger than that of the hemisphere. Thus, the current through this surface must be the same as the current leaving the sphere and therefore the current density over this electrode surface is

$$j_r = \frac{I}{2\pi r^2} = \sigma E_r \qquad (13)$$

where E_r, j_r are radial electric field and current density respectively and σ is the conductivity of the electrolyte solution.

The potential at the hemisphere is given by:

$$\varphi = -\int_{\infty}^{a} E_r \mathrm{d}r = \frac{I}{2\pi\sigma a} \qquad (14)$$

where a denotes the radius of the hemisphere, and the bulk resistance is derived based on Ohm's Law:

$$R_b = \frac{1}{2\pi\sigma a} \ [\Omega] \qquad (15)$$

Pollak (1974b) pointed out that the bulk resistance R_b is frequency-independent over a wide range (10 Hz~10 kHz used in Pollak's experiment). Myers and Saville (1989) reported the conductivity of 10^{-4} mol/L HCl was essentially constant up until 20 kHz and that the error at 200 kHz was less than 2%. Eq.(15) can be extended to include other electrode shapes of electrode by employing a shape and surface-texture multiplication factor p.

$$R_b = \frac{1}{2\pi\sigma a p} \ [\Omega] \qquad (16)$$

Simple calculation will show that p is equal to 2 for a metal sphere immersed in an electrolyte, and 1 for a hemisphere. Our experimental result for a flat-cut disk shaped electrode was close to the value of 0.66 found by Weinman and Mahler (1964). Electrode surface area A and the bulk resistance R_b are related by a simple geometrical relation, valid when the shape of the electrode-electrolyte interface is the same (Weinman and Mahler, 1964):

$$\left(\frac{R_b}{R_b'}\right)^2 = \left(\frac{A'}{A}\right) \qquad (17)$$

where A', R_b' are the electrode surface area and the bulk resistance after the change of electrode size, respectively.

It should be particularly pointed out that the change ratio of the bulk resistance is proportional to the change ratio of the dimension (not to the area) and therefore, a current change proportional to the dimension will produce the same potential at the electrode after change (not to the constant current density).

Analytical models

Unlike the electrode-electrolyte action in electrochemistry, a number of electrodes, typically 16 or more, are used in electrical impedance tomography. Some of the electrodes are used for injecting currents or voltages and the others for voltage or current measurements depending on the protocol. Eqs.(18a) to (18d) represent a mixed boundary problem (Wang *et al*., 1999).

$$\sigma\frac{\partial\phi}{\partial n}\bigg|_{\Gamma_1}=j_1(\Gamma_1),\quad \sigma\frac{\partial\phi}{\partial n}\bigg|_{\Gamma_2}=j_2(\Gamma_2) \tag{18a}$$

$$\int_{\Gamma_1}\sigma\frac{\partial\phi}{\partial n}\mathrm{d}\Gamma=I,\quad \int_{\Gamma_2}\sigma\frac{\partial\phi}{\partial n}\mathrm{d}\Gamma=-I \tag{18b}$$

$$\phi\big|_{\Gamma_n}=\text{constant}\quad (n=1,\ 2,\ ...,\ N) \tag{18c}$$

$$\frac{\partial\phi}{\partial n}\bigg|_{\Pi}=0 \tag{18d}$$

where Γ_1, Γ_2 are current driving electrode domains (for example, an electrode domain for the adjacent electrode pair strategy or a metal walled domain for conducting boundary strategy), Γ_n are metal electrodes domains and Π represents other domain at the boundary, N is number of electrodes used in the strategy.

A number of electrode modelling methods are described in the following subsections from both analytical methods, given by the simple model, the conformal mapping model and the series expansion model, and numerical methods, given by the single-node model, the gap model and the grouped-node model using the finite element method.

1. Simple model

Employing the current dipole (3-D) or the current lines (2-D) approach is a relatively straightforward method for modelling the adjacent electrode pair strategy (Barber and Brown, 1984) and conducting boundary strategy (Wang *et al*., 1994). When the point or line shaped current models were used to simulate physical electrodes, in most cases, the boundary voltages determined by the model were an acceptable representation of the measured values except in the region close to the current driven electrodes. The results simple model showed a little error at the boundary voltages. However, the potentials at the current electrode position cannot be obtained correctly because infinite values at that position are presented (Γ_1, $\Gamma_2\to 0$, $\partial\phi/\partial n\to\infty$). Also the shunting effects of large sized electrodes (Yorkey *et al*., 1985; Cheng *et al*., 1989) cannot be simulated with the simple model given in Eq.(18c).

2. Conformal mapping model

The solution of many 2-dimensional field problems is greatly facilitated by the use of complex function theory in which one can transform the geometry of a problem into a simpler geometry or into one for which the field and potential distribution is known. Because the shape or form of an infinitesimal area is preserved, these transformations are called conformal transformations. When this method can be applied, an exact solution can be obtained (Kraus, 1953). By using a double transformation procedure, Pidcock (1994) transformed a two electrode boundary model from a real domain into a simple geometry domain in order to construct a complete model. The model satisfied the boundary conditions given by Eq.(18b) and part of Eq.(18c) (only for Γ_1 and Γ_2) and therefore also satisfied condition Eq.(18a). However, since the shunting effect of the measurement electrode was not considered in his model (condition given in Eq.(18c)), he reported that "serious errors are made in these calculations once the electrodes deviate from effective point size".

3. Series expansion model

The series expansion method (SEM) is another analytical solver used to determine electric field distribution and is based on a series solution from Fourier expansion to satisfy Laplace's equation (Ider *et al*., 1990; Zhou, 1993).

The results given by the SEM model are in good agreement with data acquired from a physical vessel when the electrode width angle, β, is not large. However, the incomplete boundary conditions given in SEM model cannot be used to model large sized electrodes since the current density is not uniform at the electrode domain, and the shunting effect of large electrodes as given in Eq.(18c) cannot be simulated by the SEM model either.

4. Finite element method models

The finite element method is more applicable than the analytical models for solving such field problems with Neumann boundary conditions in electrical impedance tomography employing current injection (Yorkey, 1987; Murai and Kagawa, 1985). A number of methods were developed to simulate large size electrodes. Hua *et al*.(1993) developed the gap model taking account of skin contact impedance and Wang *et al*.(1995b) developed the grouped-node model to handle the large size of electrodes. Many approaches were developed recently (Vauhkonen *et al*., 1999).

MEASUREMENT MODELS

Effects of electrode common voltage

One of the most problematic measurement errors arises from common mode voltage (CMV) of the differential measurement because of the limited common mode voltage rejection ratio (CMRR) of the op-amps. The common mode voltage is determined from a combination of the injecting current value, the electrode impedance and the conductivity of the conductive region. The error caused by the CMV is formed from the difference between the output impedance and the mismatched input impedance of the op-amp, and the coupling components.

Besides reducing the mismatched impedance of integrated circuits to get a 'good' measurement, the best approach is to reduce the common mode voltage. A method used by Brown and Seagar (1985), is common mode voltage feedback (CMFB). However, because of the phase delay of the feedback circuit, it will cause a phase error in the demodulation and possible feedback oscillation (Murphy and Rolfe, 1988) at high frequency. In most process engineering applications, the potential reference can be obtained by directly grounding an electrical contact to the conductive medium in the process since electrical isolation is no longer necessary in most industrial applications, which is referred to as the grounded floating measurement (GFM) (Wang *et al*., 1993). The feedback path of the CMFB and GFM methods is generally through any unused electrode in contact with the conductive region.

Current source or voltage source?

Due to the presence of the double layer capacitance, the transient time is another factor, which affects the data accuracy, particularly at a fast data collection rate. Due to the large number of ON-OFF multiplexer channel operations in the DAS, the transient time has to be taken into account and becomes a key issue for maintaining the data's accuracy.

When currents are injected through the electrode-electrolyte interface, the voltage response (boundary voltage in EIT case) from the bulk resistance (refer the equivalent circuit given in Fig.4) is independent of the transient time τ_b given by a simple calculation as of Wang (1994):

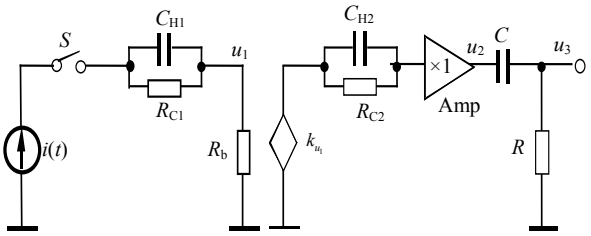

Fig.4 The equivalent circuit for one measurement channel

$$V_{R_b}(t) = I_0 R_b \tag{19a}$$

$$\tau_b = R_C C_H \tag{19b}$$

When voltages are used for injections, the response is a function with transient time τ

$$V_{R_b}(t) = V_0\left(1 - \frac{R_b}{+R_C}\right)e^{-\frac{t}{\tau_b}} + V_0\frac{R_b}{R_b + R_C} \tag{20a}$$

$$\tau_b = \frac{R_b R_C C_H}{R_C + R_b} \tag{20b}$$

Therefore, current injection is normally adopted in many measurement strategies. It should be indicated that this principle assumes that the charge and discharge process is completed before the end of pulsation and only can be applied for slow data collection speed, typically 20 frames per second.

Effect of residual potential

To analyse the effects of transient time of the sensing interface, an equivalent circuit for one conductivity measurement channel in EIT (Fig.4) was proposed by Wang *et al*.(2005). The left part of the figure is for measuring the current excitation and the right part for measuring the voltage. In the figure, $i(t)$ is a sinusoidal current source, S the switch, C_{H1}, R_{C1} the double-layer capacitance and transfer resistance of the electrode electrolyte interface at the current injection electrode, C_{H2} and R_{C2} the double-layer capacitance and transfer resistance of the electrode electrolyte interface at measurement electrode, Amp a voltage buffer with high input impedance and Gain=1, C and R the ac coupling circuit, R_b the bulk resistance of the process, k_{u_1} the transformed voltage at measurement electrode. For simplifying the discussion,

perfect sinusoidal current source and voltage buffer with infinite output and input impedances, respectively, are assumed in the model. All stray capacitances in circuits and distribution capacitances in aqueous-based process are also ignored.

Wang and Ma (2005) described the details of the transient process and reported that the response of a sensing system using switched sinusoidal current excitation is approximately the sum of an exponential term and a sinusoidal term (Eq.(21)). The exponential term is due to the discharging process of the residual potential across C_{H2}, which was charged during the previous switch operation. The value of the residual potential will be uncertain if the switch is operated randomly. The attenuation speed of the charged electrode-electrolyte interface is relatively slow (τ_2 =5 ms for example) compared with the fast frame collection rate (Δt_f<1 ms) and sampling rate of measurement (Δt_s<12.5 μs). Therefore, the residual potential could produce significant error for a fast data acquisition rate.

$$u_3(t) \approx V_{C_{H2}} e^{-t/\tau_2} + kI_m R_b \cos(\omega t + \theta) \qquad (21)$$

where θ=arctan($w\tau$), $\tau=RC$, $\tau_2=R_{C2}C_{H2}$.

To eliminate the charged potential, an over-zero switching (OZS) scheme was developed by controlling the switching phase angle of the sinusoidal current injection (Wang *et al*., 2005; Wang and Ma, 2005). Both analyses and simulation revealed that the coupling time could be dramatically reduced by the employment of the OZS scheme used now in the Leeds FIC electrical impedance camera to achieve a data acquisition speed of 1164 dual-frames (2.383 million data points) per second with a root mean square error of less than 0.6% at 80 kHz in static test application (Ma and Wang, 2004).

CONCLUSION

This paper presents full electrode models for the electrode geometry and size, the electrode-electrolyte interface and the common voltage and double-layer capacitance in measurement. Taking the full electrode models into the consideration of electrical impedance tomography would lead to further understanding of the measurement principle and optimization of the approaches to a good solution.

References

Baber, D.C., Brown, B.H., 1984. Applied potential tomography. *J. Phys. E: Sci. Instrum.*, **17**:723-733.

Bockris, J.O.M., Conway, B.E., 1969. Modern Aspects of Electrochemistry. Plenum Press, New York.

Bockris, J.O.M., Reddy, A.K.N., 1970. Modern Electrochemistry. Macdonald, London.

Bockris, J.O.M., Drazic, D.M., 1972. Electro-chemical Science. Taylor and Frabcis Ltd.

Brown, B.H., Seagar, A.D., 1985. Applied Potential Tomography: Data Collection Problems. Proc. IEE Int. Conf. on Electric and Magnetic Field in Medic. and Biolo., p.79-82.

Cheng, K., Isaacson, D., Newell, J.C., Gisser, D.C., 1989. Electrode models for electric current computed tomography. *IEEE Trans. Biom. Engng.*, **36**(9):918-924.

Cobbold, R.S.C., 1974. Transducers for Boimedical Measurements: Principles and Applications. John Wiley & Sons.

Conway, B.E., 1952. Electrochemistrical Data. Elsevier Publishing Company.

Crow, D.R., 1974. Principles and Applications of Electrochemistry. Chapman and Hall, London.

Geddes, L.A., Costa, C.P.D., Wise, G., 1971. The impedance of stainless-steel electrodes. *Med. & Biol. Engng.*, **9**:511-521.

Hua, P., Woo, E.J., Webster, J.G., Tompkins, W.J., 1993. Using compound electrodes in electrical impedance tomography. *IEEE Trans. Biomed. Eng.*, **40**(1):29-34.

Ider, Y.Z., Gencer, N.G., Altlar, E., Tosun, H., 1990. Electrical impedance tomography of translationally uniform cylidrical objects with general cross-sectional boundary. *IEEE Trans. on Med. Imag.*, **9**(1):49-59.

Kraus, J.D., 1953. Electromagnetics. Book Company, Inc.

Ma, Y., Wang, M., 2004. Performance of a High-speed Impedance Camera for Flow Informatics. Proceedings of EDSA04, ASME, Manchester.

Murphy, D., Rolfe, P., 1988. Aspects of instrumentation design for impedance imaging. *Clin. Phys. Physiol. Meas.*, **9**(A):5-14.

Murai, T., Kagawa, Y., 1985. Electrical impedance computed tomography based on a finite element model. *IEEE Trans. Biomed. Eng.*, **BME-32**(3):177-184.

Myers, D.F., Saville, D.A., 1989. Dielectric spectroscopy of colloidal suspensions. *J. Colloid and Interface Science*, **131**(2):448-460.

Pidcock, M.K., 1994. Analysing the Importance of Electrode modelling in Electrical Impedance Tomography. *In*: Beck, M.S., Campogrande, E., Morris, M., Williams, R.A., Waterfall, R.C.(Eds.), Process Tomography—A Strategy for Industrial Exploitation. UMIST, Manchester, UK, p.285-290.

Pollak, V., 1974a. An equivalent diagram for the interface impedance of metal needle electrodes. *Med. and Biolo.*

Engng., **July**:454-459.

Pollak, V., 1974b. Computation of the impedance characteristic of metal electrodes for biological investigations. *Med. and Biolo. Engng.*, **July**:460-464.

Schwan, H.P., Ferris, C.D., 1968. Four-electrode null techniques for impedance measurement with high resolution. *The Review of Scientific Instruments*, **39**(4):481-485.

Vauhkonen, P.J., Vauhkonen, M., Savolainen, T., Kaipio, P., 1999. Three-dimensional electrical impedance tomography based on the complete electrode model. *IEEE Trans. Biomed. Eng.*, **46**(9):1150-1160.

Wang, M., 1994. Electrical Impedance Tomography *n* Conducting Walled Process Vessels. Ph.D Thesis, UMIST.

Wang, M., Ma, Y.X., 2005. Over Zero Switching Scheme for Fast Data Collection Operation in Electrical Impedance Tomography. Proceedings of 4th World Congress on Industrial Process Tomography, Ajzu, Japan.

Wang, M., Dickin, F.J., Beck, M.S., 1993. Improved Electrical Impedance Tomography Data Collection System and Measurement Protocols. *In*: Beck, M.S., Campogrande, E., Morris, M., Williams, R.A., Waterfall, R.C.(Eds.), Tomography Technique and Process Design and Operation. Computational Mechanics Publications, Manchester, p.75-88.

Wang, M., Dickin, F.J., Williams, R.A., 1994. Electrical resistance tomography of metal walled vessels and pipelines. *Electronics Letters*, **30**(10):771-773.

Wang, M., Dickin, F.J., Williams, R.A., 1995a. Modelling and analysis of electrically conducting vessels and pipelines in electrical resistance process tomography. *IEE Proc. Sci. Meas. Technol.*, **142**(4):313-322.

Wang, M., Dickin, F.J., Williams, R.A., 1995b. The grouped node technique as a means of handling large electrode surfaces in electrical impedance tomography. *Physiol. Meas.*, **16**:219-226.

Wang, M., Mann, R., Dickin, F.J., 1999. Electrical resistance tomographic sensing systems for industrial applications. *Chem. Eng. Comm.*, **175**:49-70.

Wang, M., Ma, Y., Holliday, N., Dai, Y., Williams, R.A., Lucas, G., 2005. A high performance EIT system. *IEEE Sensors Journal*, **5**(2):289-299.

Weinman, J., Mahler, J., 1964. An analysis of electrical properties of metal electrodes. *Med. Electron. Biod. Engng.*, **2**:299-310.

Yorkey, T.J., Webster, J.G., Tompkins, W.J., 1985. Errors Caused by Contact Impedance in Impedance Imaging. Proc. IEEE/Seventh Ann. Conf. Eng. Med. Biol. Soc., p.632-637.

Yorkey, T.J., Webster, J.G., Tompkins, W.J., 1987. Comparing reconstruction algorithm for electrical impedance tomography. *IEEE Trans. Biomed. Eng., Nov.*, **BME-34**(11):843-851.

Zhou, P., 1993. Numerical Analysis of Electriomagnetic Fields. Springer-Verlag, Berlin, Heidelberg.